<ICCAME2022_Hogan>

Axial crushing of circular thin-walled specimens made of CFRP using progressive failure model (MAT54) in LS-Dyna

Yogesh Kumar[a,b*], Mohammad Rezasefat[c], James D. Hogan[b]

[a]*Department of Mechanical Engineering, Aligarh Muslim University (AMU), Aligarh, India 202002*
[b]*Centre for Design of Advance Materials, Department of Mechanical Engineering, University of Alberta, Edmonton, Canada AB T6G 2R3*
[c]*Politechnico di Milano, Dipartimento di Meccanica, via La Masa 1, Milano, Italy 20155*

Abstract

This research focuses on calibrating the MAT54 (ENHANCED_COMPOSITE_DAMAGE) material card in LS-Dyna for simulating axial crushing of circular thin-walled specimens made of CFRP. An IM7/8552 composite specimen showing the layup sequence of $[90_2/\pm45_2/0_2]_2$ *was simulated in LS-Dyna using shell elements. Following a trial-and-error-based method, the physical and non-physical input material parameters of MAT54 were calibrated. The calibrated input parameters included material strengths, failure strains, softening factors, and damping coefficient. The results of this study showed the applicability of the use of the physical material inputs from material characterization tests (e.g., tensile, in-plane shear, and compression) while showing the necessity of more in-depth calibration processes for the non-physical material inputs (e.g., viscous damping coefficient, crashfront reduction algorithm, etc.). The initial model predicted the specific energy absorption with an error of -57.95% and this was improved by the calibration process to an error equal to -1.49% for the final model. Now validated, the model will be used in the future to simulate impact into composite vehicle armor.*

Keywords: Axial Crushing, Composite Materials, LS-Dyna, Material calibration, Progressive failure, Finite Element Analysis

1. Introduction

Thin-walled structures made of composite materials have been widely used as energy absorbers in many engineering fields including automotive and aerospace due to their superior performance in improving the crashworthiness of structures during impact and crash situations and lightweight characteristics [1]. Energy absorber tubes made of Fibre-Reinforced Composites (FRCs) are preferred over metallic absorbers due to their higher stiffness, strength, and lower density, and this leads to a better performance in terms of energy absorption per unit mass. In addition, different failure modes such as fibre failure, delamination and matrix cracking occur during the brittle failure of composites and this contributes to their overall performance while making the design and analysis of such structures more demanding. This has led to increasing interest in the analysis and performance evaluation of composite thin-walled energy absorbers through numerical simulations [2]–[4].

The finite element method has been used previously to simulate the crushing behaviour of Carbon Fibre Reinforced Polymer (CFRP) tubes to evaluate the energy absorption performance [1]. Due to the complex constitutive behaviour of composites and their multi-mode failure behaviors, the choice of an appropriate material model is important. In the literature, several models have been developed using built-in [5]–[7] or user-defined material models [2]–[4], [8], [9] in commercial FE packages such as LS-Dyna or Abaqus. For example, Zhao et al. [2]

Corresponding Author: Yogesh Kumar
Email: yogesh3@ualberta.ca

performed a crashworthiness analysis of CFRP thin-walled structures subjected to different load cases and showed that the intralaminar failure was the dominant energy absorption mechanism during the crush event. In another study, Zhu et al. [3] investigated the energy absorption capacity of multi-cell CFRP structures under axial loading and indicated that a multi-cell structure can outperform a single-cell one. In all the studied structures, intralaminar damage was shown to be the primary failure mechanism. Liu et al. [4] investigated the effect of different tube shapes on the load bearing and failure of CFRP tubes under axial crushing. Obradovic et al. [5] studied the crash of an energy-absorbing structure made of CFRP under impact by performing simulations using MAT 54 and 55 in LS-Dyna. It was shown that simulations of energy absorbers can lead to good agreement with experimental observations even in the case of more complex geometries. Zhang et al. [6] performed an experimental and numerical analysis of Glass Fibre-Reinforced Polymer Composites (GFRP) tubes under quasi-static axial crushing. The simulations were performed in LS-Dyna using MAT 54, and this showed the capability of this material model in the prediction of the failure and mechanical response of composite tubes for crashworthiness analysis. Cherniaev et al. [7] evaluated three different material models, MAT 54, 58 and 262, in LS-Dyna for simulating the axial crushing of CFRP tubes and showed that all the material models needed extensive calibration to achieve good correlation with experimental observations. They used a trial-and-error approach for the calibration of the models. Using the material properties without tunning led to significant errors in the prediction of composite crush behaviour.

Considering the above-mentioned studies, it is concluded that the MAT54 card in LS-Dyna can be a practical tool in simulations of composite crushing. Meanwhile, the presence of a large number of input parameters, especially non-physical material inputs, necessitates more in-depth studies on the calibration of this material model. Therefore, in this paper, a trial-and-error-based approach is presented for the calibration of MAT 54 for axial crushing of CFRP IM7/8552 circular tubes. The calibration started with physical material inputs (e.g., strength and failure strain), and the non-physical inputs (e.g., softening factors and damping) are then calibrated.

2. Finite Element Modelling

2.1 Model Setup

A 3D model representing the specimen has been developed using the LS-Dyna package. The model contains three segments: the loading plate, the bevel trigger and the circular specimen. The overall length of the specimen is 200 mm as shown in Fig. 1. The loading plate was modelled using the solid elements and the MAT_RIGID material model. Material properties of the composite specimen and the loading plate are shown in Tables 1 and 2. The ELEMENT_MASS_PART card was used to replicate the 500 kN servo-hydraulic test machine with a velocity of 6 m/sec. The two-section specimen contains the bevel trigger and the circular tube which are modelled with fully integrated shell elements. The PART_COMPOSITE card is used for defining the stacking sequence of the plies within the specimen using the thickness, material angle and reference position of the integration points. The bevel trigger is simplified into reduced thickness single row shell elements. The slight taper of 0.25° for withdrawing the specimen from the mandrel in the experimental specimen was also included in the FEM study. The loading plate was assigned a constant velocity of 6 m/sec in the y-direction.

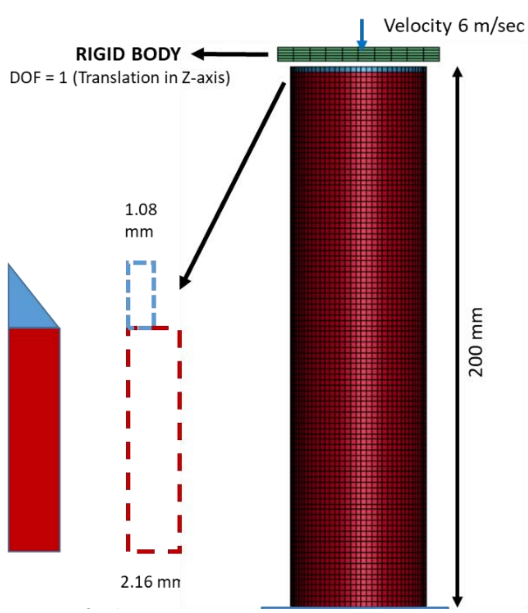

Figure 1. FEM Model of the Circular Composite Specimen.

The CONTACT_AUTOMATIC_NODES_TO_SURFACE was used to define the contact between the loading plate and the composite specimen with a coefficient of friction of 0.3. The simulation was carried out for 8.5 msec to simulate a crush length of 50 mm. The influence of the strength parameters, failure strains, and non-physical parameters like ALPHA and SOFT are analysed in this study. The Viscous Damping Coefficient (VDC) is an optional card utilized to reduce the unwanted high-frequency oscillation generated due to contact defined in case of crash tests or impact simulations [10], and it has been used in this study.

2.2 Material Modelling

For this study, a progressive failure model MAT_54_ENHANCED_COMPOSITE_DAMAGE is used for defining the orthotropic nature of the specimen. It is selected to have an economic shell-element based model while considering the individual properties of each ply [10]–[12]. MAT54 accounts for failure in tensile fiber mode, tensile matrix mode, compressive fiber mode, and compressive matrix mode with the assumption of plane stress based on the Chang-Chang failure criteria [13]. The ply is deleted on the removal of all the integration points depending on the specified failure strain defined in the material card.

Chang-Chang Failure Criteria [13], is governed by equations:

Tensile Fiber Mode ($\sigma_{11} \geq 0$)*:*

$$e_f^2 = \left(\frac{\sigma_a}{X_T}\right)^2 + \beta\left(\frac{\sigma_{ab}}{S_C}\right) - 1 \quad \begin{cases} \geq 0 \text{ failed} \\ < 0 \text{ elastic} \end{cases} \text{ if } \sigma_a > 0$$

Tensile Matrix Mode ($\sigma_{22} \geq 0$)*:*

$$e_m^2 = \left(\frac{\sigma_b}{Y_T}\right)^2 + \left(\frac{\sigma_{ab}}{S_C}\right)^2 - 1 \quad \begin{cases} \geq 0 \text{ failed} \\ < 0 \text{ elastic} \end{cases} \text{ if } \sigma_b > 0$$

Compressive Fiber Mode ($\sigma_{11} \leq 0$)*:*

$$e_c^2 = \left(\frac{\sigma_a}{X_C}\right)^2 - 1 \quad \begin{cases} \geq 0 \text{ failed} \\ < 0 \text{ elastic} \end{cases} \text{ if } \sigma_a > 0$$

Compressive Matrix Mode ($\sigma_{22} \leq 0$)*:*

$$e_d^2 = \left(\frac{\sigma_b}{2S_C}\right)^2 + \left[\left(\frac{Y_C}{2S_C}\right)^2 - 1\right]\left(\frac{\sigma_b}{Y_C}\right) + \left(\frac{\sigma_{ab}}{S_C}\right)^2 - 1 \quad \begin{cases} \geq 0 \text{ failed} \\ < 0 \text{ elastic} \end{cases} \text{ if } \sigma_b > 0$$

where *XT* and *XC* are tensile and compression in the normal direction, respectively. *YT* and *YC* are tensile and compression in the transverse direction, respectively.
The post-damage behaviour and material degradation follow the definition of the soft parameters, according to [14].
With the presence of non-physical parameters in the MAT54 material model which cannot be determined from mechanical testing, an extensive calibration of these parameters is required by a trial-and-error method [7], [15]. A sensitivity study of the various physical and non-physical parameters is performed in this investigation. The calibration scheme was initiated by exploring the dependency of the material strength properties and the degradation scheme which majorly accounts for the failure strain parameters utilized by the model. This was followed by studying the nature of non-physical parameters like the shear weighting factor and crashfront reduction factor. DATABASE_EXTENT_BINARY card is used to define the additional integration points for shell elements within the specimen to account for one integration point for each ply. When one of the failure modes is initiated from the Chang-Chang failure criteria, the strength reduction factors or damage factors get involved with the strength

material properties when the matrix starts to crack. Fiber tensile strength softening factor (FBRT) and fiber compressive strength softening factors (YCFAC) are described by the following equations:

$$X'_T = X_T \times FBRT \qquad\qquad X'_C = Y_C \times YCFAC$$

The FBRT factor ranges from 0 to 1 while, the YCFAC range depends on the compressive strength in the fiber direction and the matrix compression *XC/YC*. BETA is a shear weighting factor which influences the failure criteria in both fiber and matrix rupture by tension. In the case of Maximum shear stress failure criteria invoked by BETA = 1, the model outputs prominent behaviour in displacement values and shows the least elastic recovery [16]. To avoid this scenario of latency and more resemblance towards the experimental setup, many researchers [11], [17] have taken an equitable value of BETA = 0.5. The highly distorted unloaded elements are deleted according to the failure criteria, which requires a small timestep and this creates a significant increase in the computational cost. An additional parameter from the deck TFAIL is utilized to define the smaller step time for element deletion in the simulation and, furthermore, the crashfront algorithm will be active only when the TFAIL is greater than 0.

The deletion of the elements is also possible when the strains in each of the ply reach the failure strain parameters. These strains are defined in all in-plane directions. In the case of unidirectional tape, DFAILT and DFAILS are the tensile failure strain in fiber direction and maximum tensorial shear strain, respectively. Whereas DFAILC and DFAILM are the compressive failure strain in fiber direction and maximum strain for tensile or compressive matrix straining, respectively. Determination of these strain values has been subjective and some researchers have suggested that these can be calculated from coupon testing while [7], [18] some have extracted these parameters solely based on trial-and-error methods. In this study, we have estimated the strain values using the below-mentioned equations obtained by dividing the strength by the appropriate modulus [19].

$$DFAILT = \frac{XT}{EA} \qquad\qquad DFAILC = \frac{XC}{EA} \qquad\qquad DFAILM = \frac{(YT, YC)}{EB}$$

where *EA* and *EB* are young moduli in normal and transverse directions.
Since MAT54 only allows a single value of DFAILs to represent tensile and compressive matrix failure strain, a higher value was used for the initial baseline model. Keeping DFAILs parameters to zero will employ the Chang-Chang failure criteria for element deletion. The solver code requires the compressive strain value in negative magnitude while the tensile strain is a positive value for a successful run. In addition, the crashfront reduction factor (SOFT) reduces the strength of the elements in the next row following the deletion of the current row of elements [11]. Here, the SOFT parameter ranges from 0 to 1, where zero represents the no strength reduction in the model ahead of failure and this is highly impractical since it is a cost-efficient interpretation of the damage zone of the material. Feraboli et al. [11] describe the phenomenon as:

$$[X'_T, X'_C, Y'_T, Y'_C] = SOFT \times [X_T, X_C, Y_T, Y_C] \qquad \text{where } 0 < \text{SOFT} \leq 1$$

where X'_T, X'_C, Y'_T, Y'_C are the degraded strength parameters.
The softening factors can also be defined in the orthogonal and transverse direction by activating the SOFT2 and SOFTG parameters for the deck. MAT_20_RIGID material model was used for the simulation of the loading plate. whose properties are provided in Table 2.

Table 1. Material Properties of IM7/8552 UD Composite.

Parameters	**LS-Dyna Variables**	**Units**	**Value**	**Reference**
Density	*RO*	Kg/m^3	1610	[20]
Young's Modulus in Longitudinal Direction	*EA*	GPa	171	[18]
Young's Modulus in Transverse Direction	*EB*	GPa	8.96	[18]
Young's Modulus in Normal Direction	*EC*	GPa	8.96	[18]
Poisson's Ratio AB Direction	*PRBA*		0.32	[18]

Poisson' Ratio CA Direction	*PRCA*		0.32	[18]
Poisson' Ratio CB Direction	*PRCB*		0.5	[18]
Shear Modulus AB Direction	*GAB*	GPa	5.6	[7]
Shear Modulus BC Direction	*GBC*	GPa	2.8	[7]
Shear Modulus CA Direction	*GCA*	GPa	5.6	[7]
Longitudinal Compressive Strength	*XC*	GPa	1.59	[7]
Longitudinal Tensile Strength	*XT*	GPa	2.625	[21]
Transverse Compressive Strength	*YC*	GPa	0.3	[18]
Transverse Tensile Strength	*YT*	GPa	0.0986	[18]
Shear Strength AB Direction	*SC*	GPa	0.113	[18]

Table 2. Material Properties of Steel.

Parameters	**LS Dyna Variables**	**Units**	**Value**	**Reference**
Density	*RO*	Kg/m^3	7800	[17]
Young's Modulus	*E*	GPa	207	[17]
Poisson's Ratio	*PR*		0.33	[17]

3. Results and Discussion

3.1 Calibration of strength properties

Fig. 2a shows the effect of longitudinal compressive strength (*XC*) on the force-displacement curve. *XC* influences the peak force and the corresponding stable crushing zone. At the lower values of *XC*, the model tends to show instabilities in the later part of the curve. *XC* = 1.6 GPa is the most stabilized value when compared to others and shows more close resemblance with the experimental data [22].

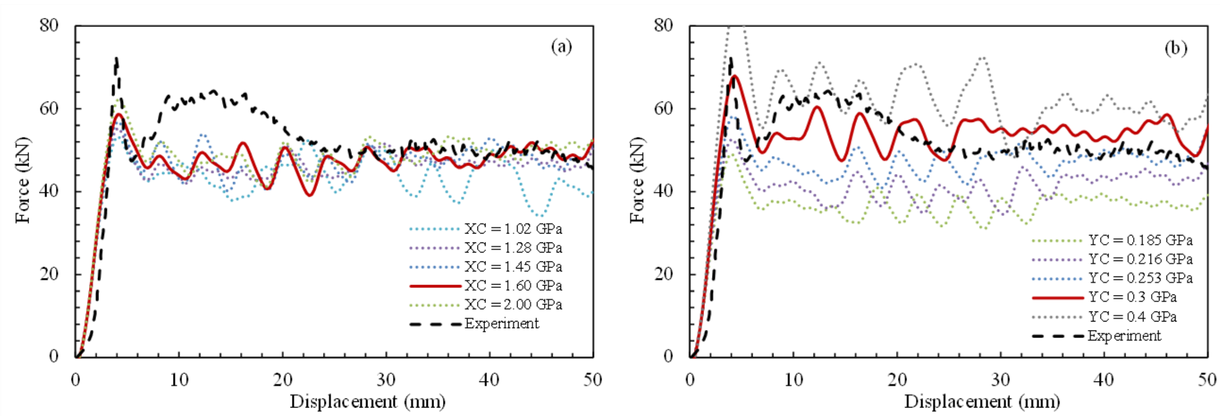

Figure 2. Variation of (a) Longitudinal Compressive Strength, and (b) Transverse Compressive Strength.

Similarly, Fig. 2 (b) shows the variation of transverse or matrix compressive strength (*YC*) on the force-displacement curve. The magnitude of the curve increases with the increase in the *YC* value, and instabilities are introduced when the value exceeds the threshold of 0.3 GPa. The results agree with the previous studies [18], [21], [23] on IM7/8552 that suggested the compressive matrix mode to be the governing failure mode for such an axial crushing scenario.

3.2 Calibration of failure strength parameters

MAT54 contains a shear failure strain parameter but it did not show any significant influence on the results. In a parametric study performed here, the obtained values from the DFAILs were further calibrated to obtain the optimum results. Fig. 3 shows the range of DFAIL parameters which were further calibrated with experimental data. The variation progressed from DFAILC, DFAILS, and DFAILT to the DFAILM. The results obtained for the DFAILC parameter indicate that the simulation is much affected by the smallest variation and hence, suggests its dominancy over the mode of failure. At DFAILC = 0.148, the Specific Energy Absorption (SEA) is 90.8 kJ/kg while the peak force tends to be 2.8% lower than the experimental value. An instability in the model was observed when the value lies below 0.10 or above 0.125, as shown in Fig. 3 (a).

At DFAILC = 0.085, the average stable crushing load was under-predicted with an error of 11.5%, while the peak force was around 20% lower than the experimental data. DFAILs above 0.125 led to over prediction of 20.6% and the average stable load was within a 16% error range. Global buckling and pre-deletion of the elements can be observed if the parameters are kept lower than 0.001. The shear strain (DFAILS) varied from 0.075 to 0.125. The iterations within the range of 0.1-0.15 showed insignificant variation in the peak force, SEA and the average stable load. However, a significant drop in the peak force and instability in the crushing zone was observed at DFAILS = 0.075. This implies that the DFAILS is not a major contributor to the overall failure when compared with the other failure modes. DFAILS = 0.118 was chosen to proceed with the calibration process as shown in Fig. 3 (b). The tensile failure strain parameter shows a minimal change in the force-displacement curve when iterated for the range of 0.085-0.120. This is obvious as the dominant failure is in compressive mode. Variations towards these parameters were simulated to fine-tune the model and understand the dependency on the failure criteria. As the DFAILT value increases, a slight increase in the peak force and average stable load was observed. No major instability was confronted within the simulated range. This records the specific energy absorption by the specimen to be 93.8 kJ/kg, which is overpredicted by a reasonable 8.26% at DFAILT = 0.115, as shown in Fig. 3 (c).

From Fig. 3 (d), it can be concluded that compression and tension failure strain (DFAILM) is one of the fundamental parameters for calibration purposes. An increase in the value directly affected the peak force and the SEA captured by the specimen. However, a value greater than 0.2 led to instability in the stable crushing zone. The model had a peak force of 76.97 kN and an average stable load of 52.07 kN at 0.178. These show strong agreement with the experimentally obtained force-displacement curves.

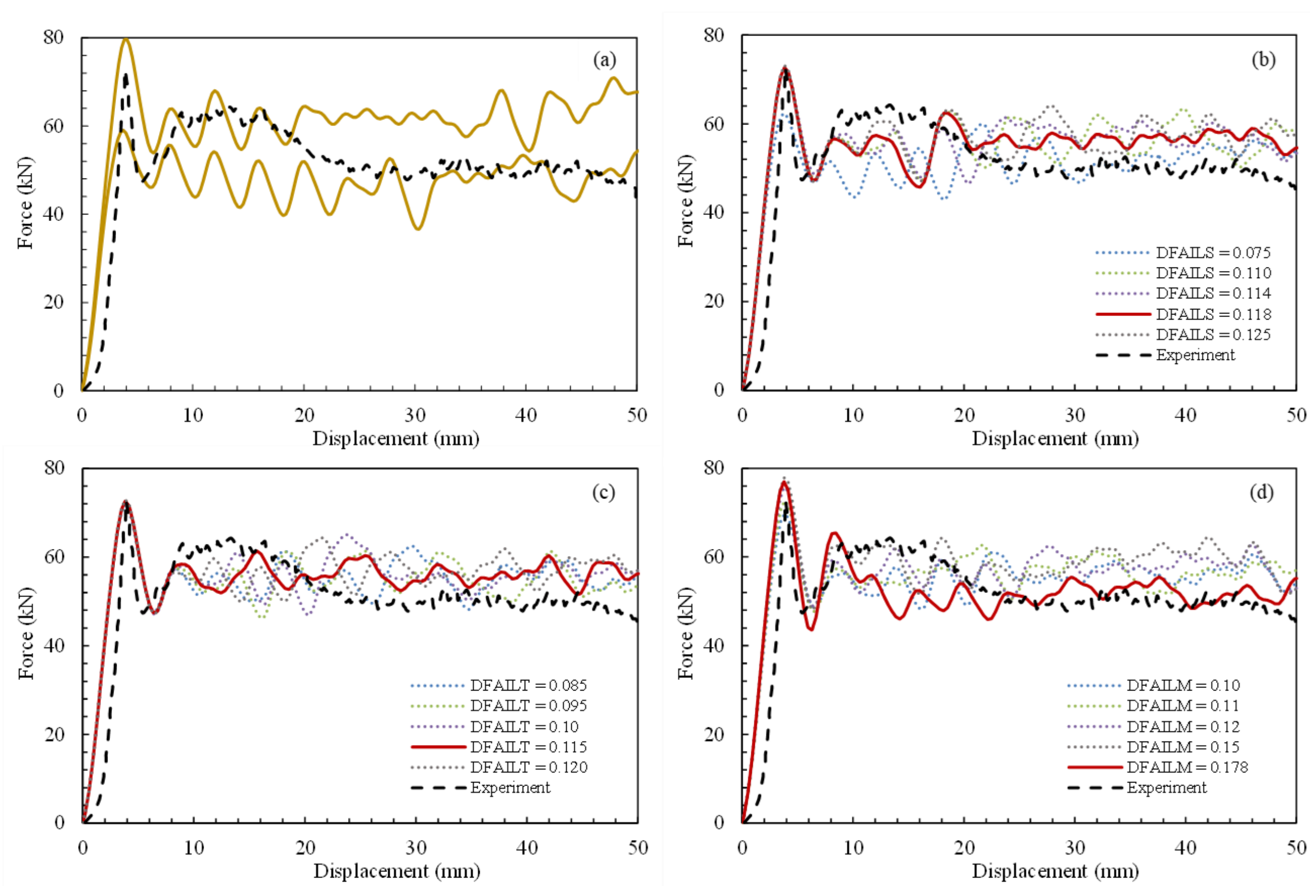

Figure 3. Variation of (a) DFAILC, (b) DFAILS, (c) DFAILT, and (d) DFAILM parameters.

3.3 Calibration of non-physical parameters

As suggested by [13], the value of VDC was kept at 40 and this corresponds to 40% of the critical damping. As can be seen in Fig. 4a, there is no significant variation in the peak force value with the change of critical damping coefficient in the range of 0-95%. However, a value over 50 led to changes in the form of over-prediction of the average stable crush load. Fig. 4b shows the effect of the non-physical parameter ALPHA which defines the non-linear shear stress term. The results confirm that the weighting factor has no influence on the force-displacement curve and the SEA captured by the specimen. However, instabilities can be observed between 15-25 mm of the crushed displacement. The post peak force curve shows similar trends to the recent study based on low-velocity impact [5]. From the literature, increasing the value of ALPHA also increases the computational time of the model.

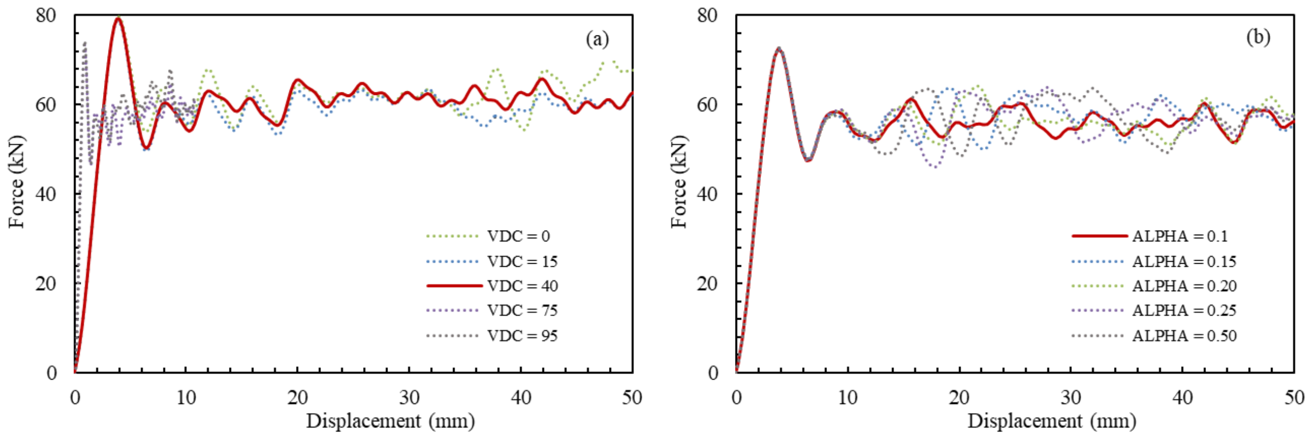

Figure 4. Variation of (a) Viscous Damping Coefficient (VDC), and (b) ALPHA parameter.

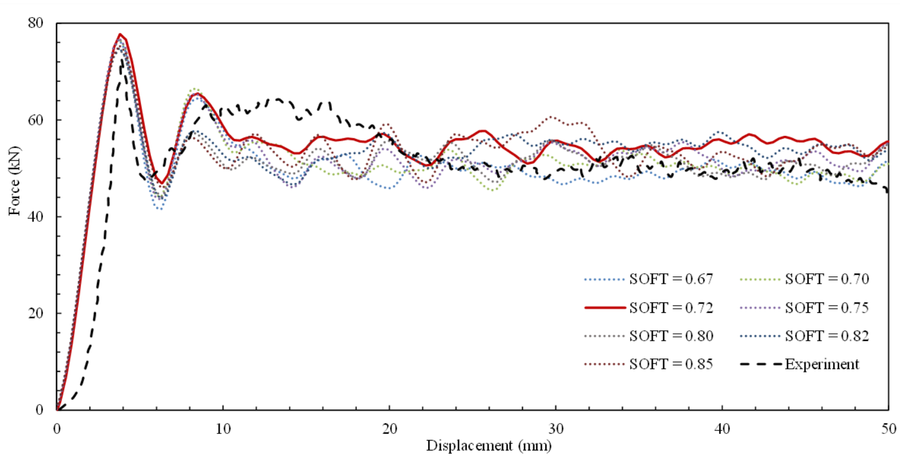

Figure 5. Variation of crashfront Reduction Factor (SOFT).

With the known brittle nature of the CFRP and the recent studies [7], [16], [17] the SOFT parameter was iterated above 0.7. SOFT is considered one of the most influential parameters as it artificially reduces the strength of the elements in the row ahead of the current crush front [17]. Fig. 5 shows the influence of the SOFT parameter on the force-displacement curve compared with the experimental data. It can be observed that only the crushing stable zone created after the failure of the trigger is influenced by this, and similar results were also observed in [16]. A value of more than 0.95 for the SOFT parameter will make the model too stiff and increases the possibility of buckling. For SOFT= 0.72, the SEA came out to be 87.90 kJ/kg with an error of +1.49% and the peak force of 76.97 kN was obtained with only a +5.85% of error. The average stable load obtained was 52.07 kN (-2.71%). Determining the correct value of the SOFT parameter needs intensive iterations based on trial-and-error method. However, the transferability of the calibration scheme with a different lay-up and ply thickness is successfully concluded in [24].

4. Conclusion

The aim of this study was to calibrate the MAT54 material model for the simulation of axial crushing of a circular cross-section tube made of CFRP. Several physical and non-physical input parameters from MAT54 were considered, including the material strengths, failure strains, softening factors, and damping coefficient. The results of the study showed that compressive fibre and matrix strength taken from tensile and compression tests led to better agreement with the experimental data, and the compressive fiber and matrix mode were the governing failure modes for axial crushing. The shear failure strain parameter did not show any influence on the simulation results, while the compressive failure strain in the fiber direction had a significant influence on the specific energy absorption of the specimen. The minimal influence of the shear strain parameter can be attributed to the dominance of fiber and matrix failure modes during the crushing [25], [26].

In addition, the damping factor of over 50% led to over prediction of the average stable crush load and a value of 40% was suggested for the simulations. Including the non-linear shear stress, behaviour showed a minor influence on the load-displacement curves while increasing the simulation time of the models. The summary of calibration process is summarized in Table 3. The calibrated model predicted the specific energy absorption with an error of -1.49% while the initial model resulted in an error of -57.95%, showing the susceptibility of MAT54 to change of the input parameters and the need for in-depth calibration scenarios.

Table 3. Energy Absorption Characterizing Parameters.

	Peak Force (kN)	Total Energy Absorbed (kN-mm)	SEA (kJ/kg)	Average Stable Load (kN)
Experiment [22]	72.71	2527.38	86.61	53.52
Initial Model	53.45	1062.72	36.42	18.49
Calibrated Model	76.97	2565.12	87.90	52.07
Error	5.85%	1.49%	1.49%	-2.70%

Acknowledgements

The authors acknowledge the support of MITACS Globalink Research Internship (GRI) program.

References

[1] A. Baroutaji, M. Sajjia, and A. G. Olabi, “On the crashworthiness performance of thin-walled energy absorbers: Recent advances and future developments,” *Thin-Walled Struct.*, vol. 118, pp. 137–163, Sep. 2017, doi: 10.1016/J.TWS.2017.05.018.

[2] X. Zhao, G. Zhu, C. Zhou, and Q. Yu, “Crashworthiness analysis and design of composite tapered tubes under multiple load cases,” *Compos. Struct.*, vol. 222, p. 110920, Aug. 2019, doi: 10.1016/J.COMPSTRUCT.2019.110920.

[3] G. Zhu, Q. Yu, X. Zhao, L. Wei, and H. Chen, “Energy-absorbing mechanisms and crashworthiness design of CFRP multi-cell structures,” *Compos. Struct.*, vol. 233, p. 111631, Feb. 2020, doi: 10.1016/J.COMPSTRUCT.2019.111631.

[4] Q. Liu, J. Ma, X. Xu, Y. Wu, and Q. Li, “Load bearing and failure characteristics of perforated square CFRP tubes under axial crushing,” *Compos. Struct.*, vol. 160, pp. 23–35, Jan. 2017, doi: 10.1016/J.COMPSTRUCT.2016.10.032.

[5] J. Obradovic, S. Boria, and G. Belingardi, “Lightweight design and crash analysis of composite frontal impact energy absorbing structures,” *Compos. Struct.*, vol. 94, no. 2, pp. 423–430, Jan. 2012, doi: 10.1016/J.COMPSTRUCT.2011.08.005.

[6] Z. Zhang, W. Sun, Y. Zhao, and S. Hou, “Crashworthiness of different composite tubes by experiments and simulations,” *Compos. Part B Eng.*, vol. 143, pp. 86–95, Jun. 2018, doi: 10.1016/J.COMPOSITESB.2018.01.021.

[7] A. Cherniaev, C. Butcher, and J. Montesano, “Predicting the axial crush response of CFRP tubes using three damage-based constitutive models,” *Thin-Walled Struct.*, vol. 129, no. February, pp. 349–364, 2018, doi:

10.1016/j.tws.2018.05.003.

[8] M. Rezasefat, A. Gonzalez-Jimenez, M. Giglio, and A. Manes, “An evaluation of Cuntze and Puck inter fibre failure criteria in simulation of thin CFRP plates subjected to low velocity impact,” *Compos. Struct.*, p. 114654, Sep. 2021, doi: 10.1016/j.compstruct.2021.114654.

[9] M. Rezasefat, A. Gonzalez-Jimenez, M. Giglio, and A. Manes, “Numerical study on the dynamic progressive failure due to low-velocity repeated impacts in thin CFRP laminated composite plates,” *Thin-Walled Struct.*, vol. 167, p. 108220, Oct. 2021, doi: 10.1016/j.tws.2021.108220.

[10] P. Feraboli, A. L. Acsl, and G. C. Llc, “Simulating Laminated Composite Materials Using LS-DYNA Material Model MAT54 : Single- Element Investigation Simulating Laminated Composite Materials Using LS-DYNA Material Model MAT54 : Single-Element Investigation,” no. December, 2017.

[11] P. Feraboli, B. Wade, F. Deleo, M. Rassaian, M. Higgins, and A. Byar, “LS-DYNA MAT54 modeling of the axial crushing of a composite tape sinusoidal specimen,” *Compos. Part A Appl. Sci. Manuf.*, vol. 42, no. 11, pp. 1809–1825, 2011, doi: 10.1016/j.compositesa.2011.08.004.

[12] P. Feraboli, “Development of a corrugated test specimen for composite materials energy absorption,” *J. Compos. Mater.*, vol. 42, no. 3, pp. 229–256, 2008, doi: 10.1177/0021998307086202.

[13] F. Chang and K. Chang, “A Progressive Damage Model for Laminated Composites Containing Stress Concentrations,” *J. Compos. Mater.*, vol. 21, no. September, pp. 834–855, 1987, doi: https://doi.org/10.1177/002199838702100904.

[14] Livermore Software Technology Corporation (LSTC), *Keyword User’s Manual Volume 1*, vol. I. 2014.

[15] W. Bonnie and P. Faraboli, “Crushing Behavior of Laminated Composite Structural Elements : Experiment and LS-DYNA Simulation,” 2016.

[16] F. Vannucchi de Camargo, A. Pavlovic, E. C. Schenal, and C. Fragassa, “Explicit Stacked-Shell Modelling of Aged Basalt Fiber Reinforced Composites to Low-Velocity Impact,” *Compos. Struct.*, 2021, doi: 10.1016/j.compstruct.2020.113017.

[17] A. Cherniaev, J. Montesano, and C. Butcher, “Modeling the Axial Crush Response of CFRP Tubes using MAT 054, MAT058 and MAT262 in LS-DYNA,” *15th Int. LS-DYNA Users Conf.*, pp. 1–17, 2018.

[18] Y. Nikishkov, A. Makeev, and G. Seon, “Progressive fatigue damage simulation method for composites,” *Int. J. Fatigue*, vol. 48, pp. 266–279, 2013, doi: 10.1016/j.ijfatigue.2012.11.005.

[19] M. Osborne, “Single-Element Characterization of the LS-DYNA MAT54 Material Model,” p. 113, 2012.

[20] H. Koerber *et al.*, “Experimental characterization and constitutive modeling of the non-linear stress–strain behavior of unidirectional carbon–epoxy under high strain rate loading,” *Adv. Model. Simul. Eng. Sci.*, vol. 5, no. 1, 2018, doi: 10.1186/s40323-018-0111-x.

[21] H. Cui, D. Thomson, S. Eskandari, and N. Petrinic, “A critical study on impact damage simulation of IM7/8552 composite laminate plate,” *Int. J. Impact Eng.*, vol. 127, no. October 2018, pp. 100–109, 2019, doi: 10.1016/j.ijimpeng.2019.01.009.

[22] Marc A. Courteau, “Investigating the Crashworthiness Characteristics of Carbon Fiber/Epoxy Tubes,” University of Utah, 2011.

[23] J. Reiner and R. Vaziri, “Progressive axial crushing of composite laminates: A comparison between LS-DYNA continuum damage models,” *33rd Tech. Conf. Am. Soc. Compos. 2018*, vol. 3, no. November, pp. 2048–2058, 2018, doi: 10.12783/asc33/26071.

[24] C. Reuter, K. H. Sauerland, and T. Tröster, “Experimental and numerical crushing analysis of circular CFRP tubes under axial impact loading,” *Compos. Struct.*, 2017, doi: 10.1016/j.compstruct.2017.04.052.

[25] S. Boria, “Sensitivity Analysis of Material Model Parameters to Reproduce Crushing of Composite Tubes,” *J. Mater. Eng. Perform.*, vol. 28, no. 6, pp. 3267–3280, 2019, doi: 10.1007/s11665-019-04047-6.

[26] Y. Ren, H. Jiang, B. Gao, and J. Xiang, “A progressive intraply material deterioration and delamination based failure model for the crashworthiness of fabric composite corrugated beam: Parameter sensitivity analysis,” *Compos. Part B Eng.*, vol. 135, pp. 49–71, 2018, doi: 10.1016/j.compositesb.2017.09.072.